Journal of Geophysical Research - Planets

Supporting Information for

Chromium on Mercury: New results from the MESSENGER X-Ray Spectrometer and implications for the innermost planet's geochemical evolution

Larry R. Nittler[1,2*], Asmaa Boujibar[1,3], Ellen Crapster-Pregont[4,5], Elizabeth A. Frank[1], Timothy J. McCoy[6], Francis M. McCubbin[7], Richard D. Starr[8,9], Audrey Vorburger[4,10], Shoshana Z. Weider[1,11]

[1]Earth and Planets Laboratory, Carnegie Institution of Washington, Washington, DC, USA
[2]School of Earth and Space Exploration, Arizona State University, Tempe, AZ, USA
[3]Geology Department, Department of Physics & Astronomy, Western Washington University, Bellingham, WA, USA
[4]Department of Earth and Planetary Sciences, American Museum of Natural History, New York, NY, USA
[5]Department of Earth and Environmental Sciences, Columbia University, New York, NY, USA
[6]National Museum of Natural History, Smithsonian Institution, Washington, DC, USA,
[7]Astromaterials Research and Exploration Science Division, NASA Johnson Space Center, Houston, TX, USA
[8]Physics Department, The Catholic University of America, Washington, DC, USA
[9]Solar System Exploration Division, NASA Goddard Space Flight Center, Greenbelt, MD, USA,
[10]Physics Institute, University of Bern, Bern, Switzerland
[11]Agile Decision Services, Washington, DC, USA
*Corresponding author, lnittler@asu.edu.

Contents of this file

Text S1
Figures S1 and S2
Table S1
References

Additional Supporting Information (Files uploaded separately)

Maps.zip This is a zip archive containing 18 images (*.png) giving mapped Mg/Si, Al/Si and Cr/Si elemental abundance data on Mercury as shown graphically in Figure 3 as well as **Maps-README.txt**, a text file describing the *.png files.

crflaredata.csv: a table in comma-separated-variables format of fitting results for the 133 MESSENGER XRS flare data used in the paper. Cr/Si and Fe/Si ratios are corrected for the phase angle effect, as discussed in the paper. Both corrected and uncorrected data are provided for Cr/Si. Error bars are one-sigma. Errors are statistical and systematic error bars may be larger. Columns are defined as follows:

Flare: a number label for each record

STARTMET: Mission elapsed time (MET) of the first MXRS data record used for spectral sum. MET isseconds since launch of spacecraft.

ENDMET: Mission elapsed time (MET) of the last MXRS data record used for spectral sum. MET isseconds since launch of spacecraft.

START UTC: Date and time (in UTC) of the first MXRS data record used for spectral sum

END UTC: Date and time (in UTC) of the last MXRS data record used for spectral sum

PPLOTINCLUDE: If this variable is set to 1, this flare result was included in the calculation of phase angle correction and plotted in Figure 2

Area (km2): The total area of XRS footprint over spectral integration in square kilometers.

FPASPECT A unitless parameter that gives a rough measure of how asymmetric the XRS footprint is (high means stretched N-S, lower than 1 means stretched E-W); see L. R. Nittler et al., "Global major-element maps of Mercury from four years of MESSENGER X-Ray Spectrometer observations," Icarus, vol. 345, p. 113716, Jul. 2020, doi: 10.1016/j.icarus.2020.113716.

Latitude: average latitude of the XRS footprint for the spectra integration.

Longitude: average latitude of the XRS footprint for the spectra integration.

Incidence angle (deg): Average incidence (sun-surface normal) angle, in degrees, averaged over XRS footprint for spectral integration

Emission angle (deg): Average emission (XRS-surface normal) angle, in degrees, averaged over XRS footprint for spectral integration

Phase angle (deg): Average phase (spacecraft-surface-sun) angle, in degrees, averaged over XRS footprint for spectral integration

Solar temp (MK): Estimated average temperature of solar corona (in millions of kelvin) inferred from MESSENGER X-ray Solar Monitor measurement acquired at same time as spectral measurement

Mg/Si: Mg/Si weight ratio determined from fitting of spectral integration

er Mg/Si: One-sigma statistical error of Mg/Si weight ratio determined from fitting of spectral integration

Al/Si: Al/Si weight ratio determined from fitting of spectral integration

er Al/Si: One-sigma statistical error of Al/Si weight ratio determined from fitting of spectral integration

S/Si: S/Si weight ratio determined from fitting of spectral integration

er S/Si: One-sigma statistical error of S/Si weight ratio determined from fitting of spectral integration

Ca/Si: Ca/Si weight ratio determined from fitting of spectral integration

er Ca/Si: One-sigma statistical error of Ca/Si weight ratio determined from fitting of spectral integration

Ti/Si: Ti/Si weight ratio determined from fitting of spectral integration

er Al/Si: One-sigma statistical error of Ti/Si weight ratio determined from fitting of spectral integration

Cr/Si (not phase corrected): Cr/Si weight ratio determined from fitting of spectral integration (not phase corrected)

er Cr/Si (not phase corrected): One-sigma statistical error of Cr/Si weight ratio determined from fitting of spectral integration(not phase corrected)

Cr/Si (phase corrected): Cr/Si weight ratio determined from fitting of spectral integration (phase corrected)

er Cr/Si (phase corrected): One-sigma statistical error of Cr/Si weight ratio determined from fitting of spectral integration (not phase corrected)

Fe/Si: Fe/Si weight ratio determined from fitting of spectral integration (phase-corrected)

er Fe/Si: One-sigma statistical error of Fe/Si weight ratio determined from fitting of spectral integration (phase-corrected)

Introduction

This document includes two supplementary figures referred to in the text and a table providing the literature references for the experimental partitioning data used in the manuscript (for example in Figures 6 and 7). Additional supplementary information included are:

Text S1.

To construct a model predicting metal silicate partitioning of Cr, we performed a linear regression using 520 experimental data from 43 peer-reviewed publications (Ballhaus et al., 2013; Berthet et al., 2009; Boujibar et al., 2014, 2016, 2019, 2020; Cartier et al., 2020; Cartier, Hammouda, Boyet, et al., 2014; Cartier, Hammouda, Doucelance, et al., 2014; Chabot & Agee, 2003; Clesi et al., 2016; Corgne et al., 2008; C.R.M. Jackson et al., 2021; Dasgupta et al., 2013; Fischer et al., 2015, 2020; Geßmann & Rubie, 1998; Hiligren et al., 1994; Huang et al., 2020, 2021; Jana & Walker, 1997; Jennings et al., 2021; Kaaden & McCubbin, 2016; Kilburn & Wood, 1997; Laurenz et al., 2016; Malavergne et al., 2019; Mann et al., 2009, 2012; Righter et al., 2010, 2018; Siebert et al., 2011, 2012; Steenstra et al., 2017, 2018; Steenstra, Seegers, et al., 2020; Steenstra, Trautner, et al., 2020; Thibault & Walter, 1995; Tuff et al., 2011; Wade & Wood, 2001, 2005; Walker et al., 1993; Wood et al., 2008, 2014). Similarly, to model Cr partitioning between sulfide and silicate, we used a compilation of 253 experimental data from 17 peer-reviewed publications (Berthet et al., 2009; Boujibar et al., 2014, 2019, 2020; Cartier et al., 2020; Jana & Walker, 1997; Kaaden & McCubbin, 2016; Kiseeva & Wood, 2015; Laurenz et al., 2016; Mann et al., 2009; Namur et al., 2016; Steenstra et al., 2017, 2018; Steenstra, Haaster, et al., 2020; Walker et al., 1993; Wood et al., 2014). In the table S1 below we show these references in a table with additional information on C concentration used for modeling (see main text for more detail).

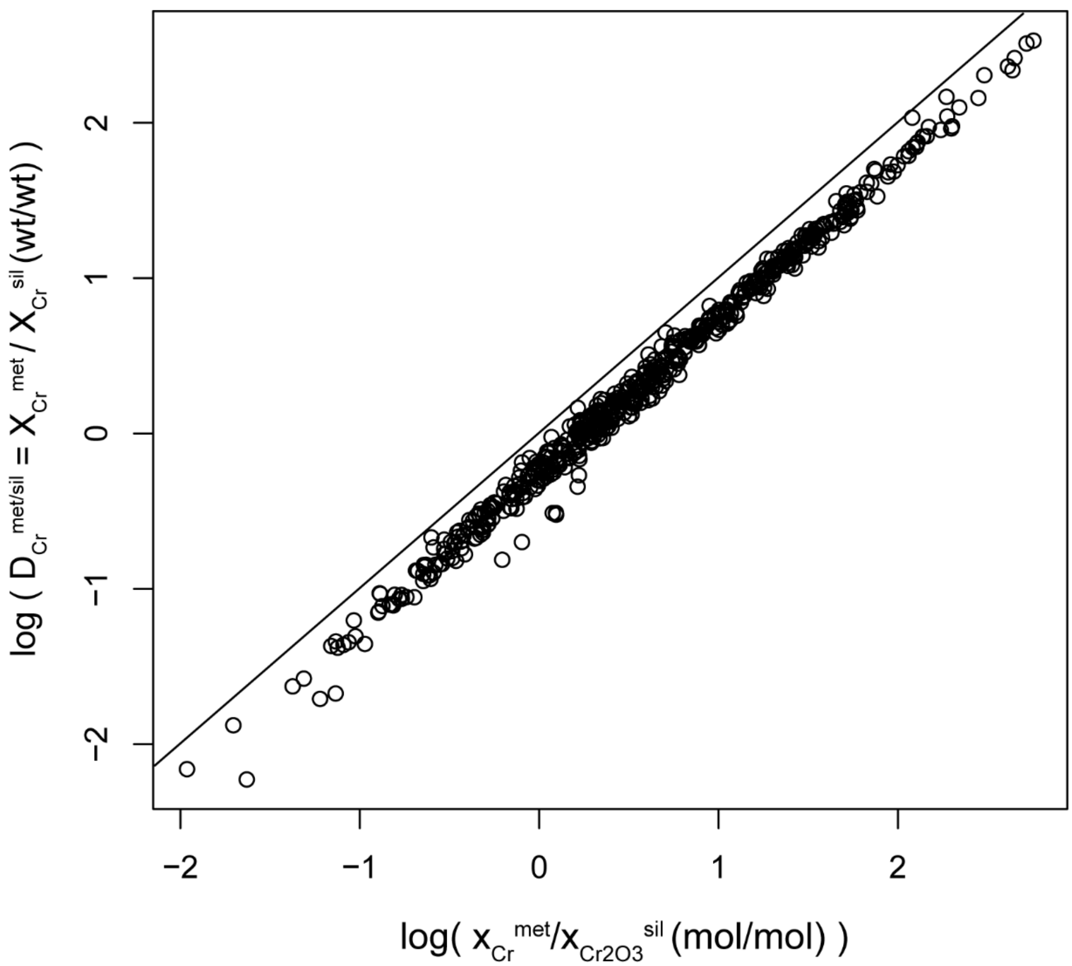

Figure S1. Comparison between the experimental Nernst partition coefficients $X_{Cr}^{met}/X_{Cr}^{sil}$ (wt/wt) with the molar $x_{Cr}^{met}/x_{Cr2O3}^{sil}$ partition coefficients. The black line represents y=x. The linear relationship between the log of both Cr partition coefficients calculated in these two different ways allows to model Nernst Cr partition coefficient using the equation (3) (see main text for more details).

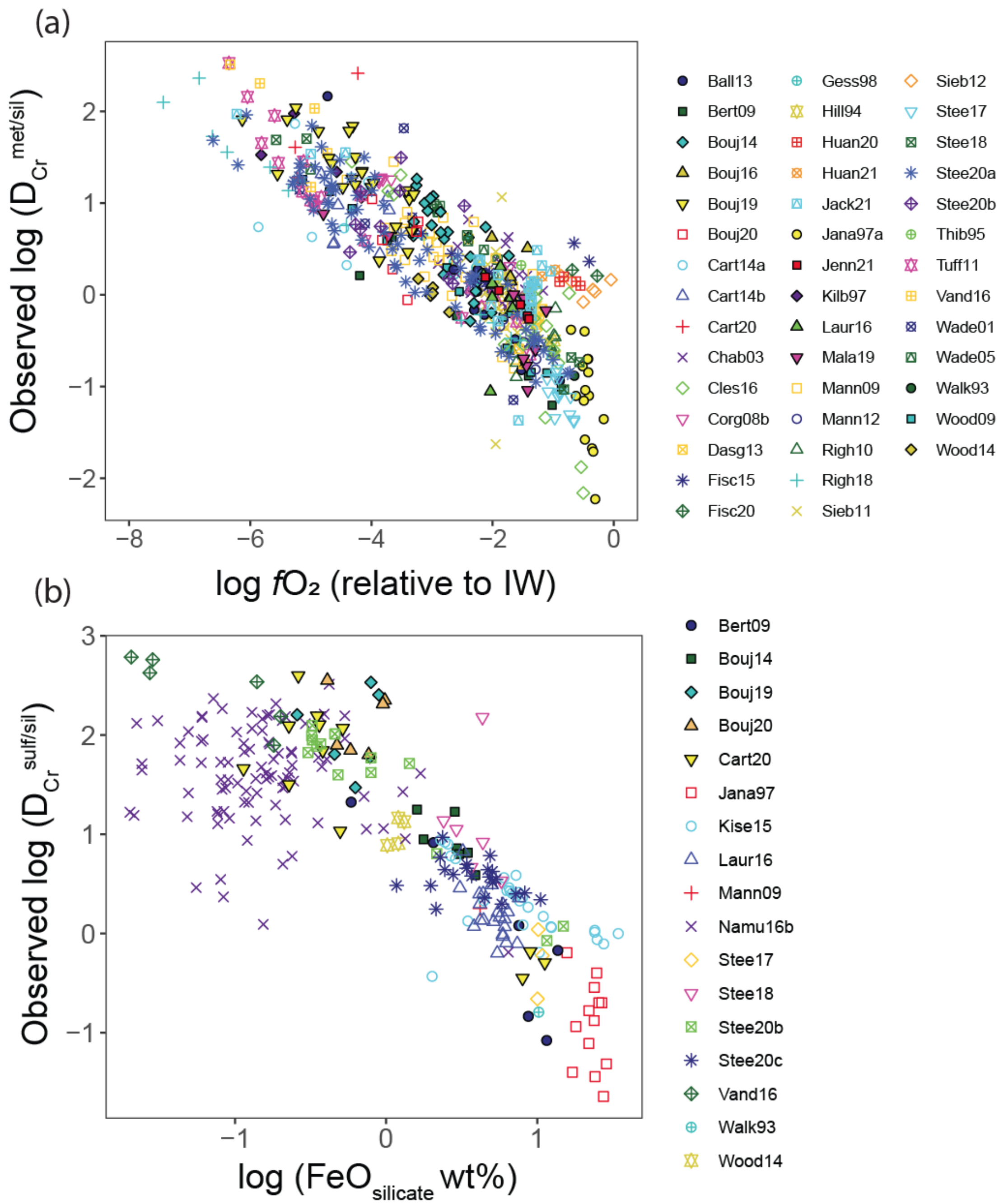

Figure S2. (a) Same as Figure 6b of Main Text, only with symbols indicating literature source of data points (Table S1). (b) Same as Figure 7b of Main Text, only with symbols indicating literature source of data points (Table S1).

Table S1. List of references for experimental data used in paper; codes are indicated on Figures 6, 7, and S2. A “*” following a reference indicates publications where experiments using graphite capsules have not measured C concentration in the metallic phase. In these experiments, C concentration was estimated by subtracting the sum of all other elemental concentrations from 100 wt%. The complete reference list can be found below at the end of this document.

Metal-Silicate		Sulfide-silicate	
Code	Reference	Code	Reference
Ball13	Ballhaus et al. 2013	Bert09	Berthet et al. 2009*
Bert09	Berthet et al.2009*	Bouj14	Boujibar et al. 2014
Bouj14	Boujibar et al. 2014	Bouj19	Boujibar et al. 2019
Bouj16	Boujibar et al. 2016*	Bouj20	Boujibar et al. 2020
Bouj19	Boujibar et al. 2019	Cart20	Cartier et al. 2020*
Bouj20	Boujibar et al. 2020	Jana97	Jana & Walker 1997*
Cart14a	Cartier et al. 2014a*	Kise15	Kiseeva & Wood 2015*
Cart14b	Cartier et al. 2014b*	Laur16	Laurenz et al. 2016
Cart20	Cartier et al. 2020*	Mann09	Mann et al. 2009*
Chab03	Chabot & Agee 2003*	Namu16b	Namur et al. 2016*
Cles16	Clesi et al. 2016*	Stee17	Steenstra et al. 2017
Corg08b	Corgne et al. 2008	Stee18	Steenstra et al. 2018*
Dasg13	Dasgupta et al. 2013	Stee20b	Steenstra et al. 2020c*
Fisc15	Fischer et al. 2015	Stee20c	Steenstra et al. 2020b*
Fisc20	Fischer et al. 2020	Vand16	Vander Kaaden & McCubbin 2016*
Gess98	Gessmann and Rubie 1998	Walk93	Walker et al. 1993*
Hill94	Hillgren et al. 1994	Wood14	Wood et al. 2014
Huan20	Huang et al. 2020		
Huan21	Huang et al. 2021		
Jack21	Jackson et al. 2021		
Jana97a	Jana & Walker 1997*		
Jenn21	Jennings et al. 2021		
Kilb97	Kilburn & Wood 1997		
Laur16	Laurenz et al. 2016		
Mala19	Malavergne et al. 2019*		
Mann09	Mann et al. 2009*		
Mann12	Mann et al. 2012		
Righ10	Righter et al. 2010		
Righ18	Righter et al. 2018		
Sieb11	Siebert et al. 2011*		
Sieb12	Siebert et al. 2012		
Stee17	Steenstra et al. 2017		
Stee18	Steenstra et al. 2018*		

Stee20a	Steenstra et al. 2020a*		
Stee20b	Steenstra et al. 2020b*		
Thib95	Thibault & Walter 1995*		
Tuff11	Tuff et al. 2011		
Vand16	Vander Kaaden & McCubbin 2016*		
Wade01	Wade & Wood 2001		
Wade05	Wade & Wood 2005*		
Walk93	Walker et al. 1993*		
Wood09	Wood et al. 2009		
Wood14	Wood et al. 2014		

References

Ballhaus, C., Laurenz, V., Münker, C., Fonseca, R. O. C., Albarède, F., Rohrbach, A., Lagos, M., Schmidt, M. W., Jochum, K.-P., Stoll, B., Weis, U., & Helmy, H. M. (2013). The U/Pb ratio of the Earth's mantle—A signature of late volatile addition. *Earth and Planetary Science Letters*, *362*, 237–245. https://doi.org/10.1016/j.epsl.2012.11.049

Berthet, S., Malavergne, V., & Righter, K. (2009). Melting of the Indarch meteorite (EH4 chondrite) at 1GPa and variable oxygen fugacity: Implications for early planetary differentiation processes. *Geochimica et Cosmochimica Acta*, *73*(20), 6402–6420. https://doi.org/10.1016/j.gca.2009.07.030

Boujibar, A., Andrault, D., Bouhifd, M. A., Bolfan-Casanova, N., Devidal, J.-L., & Trcera, N. (2014). Metal–silicate partitioning of sulphur, new experimental and thermodynamic constraints on planetary accretion. *Earth and Planetary Science Letters*, *391*, 42–54. https://doi.org/10.1016/j.epsl.2014.01.021

Boujibar, A., Bolfan-Casanova, N., Andrault, D., Bouhifd, M. A., & Trcera, N. (2016). Incorporation of Fe2+ and Fe3+ in bridgmanite during magma ocean crystallization. *American Mineralogist*, *101*(7), 1560–1570. https://doi.org/doi:10.2138/am-2016-5561

Boujibar, A., Habermann, M., Righter, K., Ross, D. K., Pando, K., Righter, M., Chidester, B. A., & Danielson, L. R. (2019). U, Th, and K partitioning between metal, silicate, and sulfide and implications for Mercury's structure, volatile content, and radioactive heat production. *American Mineralogist*, *104*(9), 1221–1237. https://doi.org/doi:10.2138/am-2019-7000

Boujibar, A., Righter, K., Bullock, E. S., Du, Z., & Fei, Y. (2020). Segregation of Na, K, Rb and Cs into the cores of Earth, Mars and Vesta constrained with partitioning experiments. *Geochimica et Cosmochimica Acta*, *269*, 622–638. https://doi.org/10.1016/j.gca.2019.11.014

Cartier, C., Hammouda, T., Boyet, M., Bouhifd, M. A., & Devidal, J.-L. (2014). Redox control of the fractionation of niobium and tantalum during planetary accretion and core formation. *Nature Geoscience*, *7*(8), 573–576. https://doi.org/10.1038/ngeo2195

Cartier, C., Hammouda, T., Doucelance, R., Boyet, M., Devidal, J.-L., & Moine, B. (2014). Experimental study of trace element partitioning between enstatite and melt in enstatite chondrites at low oxygen fugacities and 5GPa. *Geochimica et Cosmochimica Acta*, *130*, 167–187. https://doi.org/10.1016/j.gca.2014.01.002

Cartier, C., Namur, O., Nittler, L. R., Weider, S. Z., Crapster-Pregont, E., Vorburger, A., Frank, E. A., & Charlier, B. (2020). No FeS layer in Mercury? Evidence from Ti/Al measured by MESSENGER. *Earth and Planetary Science Letters*, *534*, 116108. https://doi.org/10.1016/j.epsl.2020.116108

Chabot, N. L., & Agee, C. B. (2003). Core formation in the Earth and Moon: New experimental constraints from V, Cr, and Mn. *Geochimica et Cosmochimica Acta*, *67*(11), 2077–2091. https://doi.org/10.1016/S0016-7037(02)01272-3

Clesi, V., Bouhifd, M. A., Bolfan-Casanova, N., Manthilake, G., Fabbrizio, A., & Andrault, D. (2016). Effect of H2O on metal–silicate partitioning of Ni, Co, V, Cr, Mn and Fe: Implications for the oxidation state of the Earth and Mars. *Geochimica et Cosmochimica Acta*, *192*, 97–121. https://doi.org/10.1016/j.gca.2016.07.029

Corgne, A., Keshav, S., Wood, B. J., McDonough, W. F., & Fei, Y. (2008). Metal–silicate partitioning and constraints on core composition and oxygen fugacity during Earth accretion. *Geochimica et Cosmochimica Acta*, *72*(2), 574–589. https://doi.org/10.1016/j.gca.2007.10.006

C.R.M. Jackson, E. Cottrell, Z. Du, N.R. Bennett, & Y. Fei. (2021). High pressure redistribution of nitrogen and sulfur during planetary stratification. *Geochemical Perspectives Letters*, *18*, 37–42. https://doi.org/10.7185/geochemlet.2122

Dasgupta, R., Chi, H., Shimizu, N., Buono, A. S., & Walker, D. (2013). Carbon solution and partitioning between metallic and silicate melts in a shallow magma ocean: Implications for the origin and distribution of terrestrial carbon. *Geochimica et Cosmochimica Acta*, *102*, 191–212. https://doi.org/10.1016/j.gca.2012.10.011

Fischer, R. A., Cottrell, E., Hauri, E., Lee, K. K. M., & Voyer, M. L. (2020). The carbon content of Earth and its core. *Proceedings of the National Academy of Sciences*, *117*(16), 8743–8749. https://doi.org/10.1073/pnas.1919930117

Fischer, R. A., Nakajima, Y., Campbell, A. J., Frost, D. J., Harries, D., Langenhorst, F., Miyajima, N., Pollok, K., & Rubie, D. C. (2015). High pressure metal–silicate partitioning of Ni, Co, V, Cr, Si, and O. *Geochimica et Cosmochimica Acta*, *167*, 177–194. https://doi.org/10.1016/j.gca.2015.06.026

Geßmann, C. K., & Rubie, D. C. (1998). The Effect of Temperature on the Partitioning of Nickel, Cobalt, Manganese, Chromium, and Vanadium at 9 GPa and Constraints on Formation of the Earth's Core. *Geochimica et Cosmochimica Acta*, *62*(5), 867–882. https://doi.org/10.1016/S0016-7037(98)00023-4

Hiligren, V. J., Drake, M. J., & Rubie, D. C. (1994). High-Pressure and High-Temperature Experiments on Core-Mantle Segregation in the Accreting Earth. *Science*, *264*(5164), 1442–1445. https://doi.org/10.1126/science.264.5164.1442

Huang, D., Badro, J., & Siebert, J. (2020). The niobium and tantalum concentration in the mantle constrains the composition of Earth's primordial magma ocean. *Proceedings of the National Academy of Sciences*, *117*(45), 27893–27898. https://doi.org/10.1073/pnas.2007982117

Huang, D., Siebert, J., & Badro, J. (2021). High pressure partitioning behavior of Mo and W and late sulfur delivery during Earth's core formation. *Geochimica et Cosmochimica Acta*, *310*, 19–31. https://doi.org/10.1016/j.gca.2021.06.031

Jana, D., & Walker, D. (1997). The influence of sulfur on partitioning of siderophile elements. *Geochimica et Cosmochimica Acta*, *61*(24), 5255–5277. https://doi.org/10.1016/S0016-7037(97)00307-4

Jennings, E. S., Jacobson, S. A., Rubie, D. C., Nakajima, Y., Vogel, A. K., Rose-Weston, L. A., & Frost, D. J. (2021). Metal–silicate partitioning of W and Mo and the role of carbon in controlling their abundances in the bulk silicate earth. *Geochimica et Cosmochimica Acta*, *293*, 40–69. https://doi.org/10.1016/j.gca.2020.09.035

Kaaden, K. E. V., & McCubbin, F. M. (2016). The origin of boninites on Mercury: An experimental study of the northern volcanic plains lavas. *Geochimica et Cosmochimica Acta*, *173*, 246–263. https://doi.org/10.1016/j.gca.2015.10.016

Kilburn, M. R., & Wood, B. J. (1997). Metal–silicate partitioning and the incompatibility of S and Si during core formation. *Earth and Planetary Science Letters*, *152*(1), 139–148. https://doi.org/10.1016/S0012-821X(97)00125-8

Kiseeva, E. S., & Wood, B. J. (2015). The effects of composition and temperature on chalcophile and lithophile element partitioning into magmatic sulphides. *Earth and Planetary Science Letters*, *424*, 280–294. https://doi.org/10.1016/j.epsl.2015.05.012

Laurenz, V., Rubie, D. C., Frost, D. J., & Vogel, A. K. (2016). The importance of sulfur for the behavior of highly-siderophile elements during Earth's differentiation. *Geochimica et Cosmochimica Acta*, *194*, 123–138. https://doi.org/10.1016/j.gca.2016.08.012

Malavergne, V., Bureau, H., Raepsaet, C., Gaillard, F., Poncet, M., Surblé, S., Sifré, D., Shcheka, S., Fourdrin, C., Deldicque, D., & Khodja, H. (2019). Experimental constraints on the fate of H and C during planetary core-mantle differentiation. Implications for the Earth. *Icarus*, *321*, 473–485. https://doi.org/10.1016/j.icarus.2018.11.027

Mann, U., Frost, D. J., & Rubie, D. C. (2009). Evidence for high-pressure core-mantle differentiation from the metal–silicate partitioning of lithophile and weakly-siderophile elements. *Geochimica et Cosmochimica Acta*, *73*(24), 7360–7386. https://doi.org/10.1016/j.gca.2009.08.006

Mann, U., Frost, D. J., Rubie, D. C., Becker, H., & Audétat, A. (2012). Partitioning of Ru, Rh, Pd, Re, Ir and Pt between liquid metal and silicate at high pressures and high temperatures—Implications for the origin of highly siderophile element concentrations in the Earth's mantle. *Geochimica et Cosmochimica Acta*, *84*, 593–613. https://doi.org/10.1016/j.gca.2012.01.026

Namur, O., Charlier, B., Holtz, F., Cartier, C., & McCammon, C. (2016). Sulfur solubility in reduced mafic silicate melts: Implications for the speciation and distribution of sulfur on Mercury. *Earth and Planetary Science Letters*, *448*, 102–114. https://doi.org/10.1016/j.epsl.2016.05.024

Righter, K., Pando, K., Humayun, M., Waeselmann, N., Yang, S., Boujibar, A., & Danielson, L. R. (2018). Effect of silicon on activity coefficients of siderophile elements (Au, Pd, Pt, P, Ga, Cu, Zn, and Pb) in liquid Fe: Roles of core formation, late sulfide matte, and late veneer in shaping terrestrial mantle geochemistry. *Geochimica et Cosmochimica Acta*, *232*, 101–123. https://doi.org/10.1016/j.gca.2018.04.011

Righter, K., Pando, K. M., Danielson, L., & Lee, C.-T. (2010). Partitioning of Mo, P and other siderophile elements (Cu, Ga, Sn, Ni, Co, Cr, Mn, V, and W) between metal and silicate melt as a function of temperature and silicate melt composition. *Earth and Planetary Science Letters*, *291*(1), 1–9. https://doi.org/10.1016/j.epsl.2009.12.018

Siebert, J., Badro, J., Antonangeli, D., & Ryerson, F. J. (2012). Metal–silicate partitioning of Ni and Co in a deep magma ocean. *Earth and Planetary Science Letters*, *321–322*, 189–197. https://doi.org/10.1016/j.epsl.2012.01.013

Siebert, J., Corgne, A., & Ryerson, F. J. (2011). Systematics of metal–silicate partitioning for many siderophile elements applied to Earth's core formation. *Geochimica et Cosmochimica Acta*, *75*(6), 1451–1489. https://doi.org/10.1016/j.gca.2010.12.013

Steenstra, E. S., Agmon, N., Berndt, J., Klemme, S., Matveev, S., & van Westrenen, W. (2018). Depletion of potassium and sodium in mantles of Mars, Moon and Vesta by core formation. *Scientific Reports*, *8*(1), 7053. https://doi.org/10.1038/s41598-018-25505-6

Steenstra, E. S., Haaster, F. van, Mulligen, R. van, Flemetakis, S., Berndt, J., Klemme, S., & Westrenen, W. van. (2020). An experimental assessment of the chalcophile behavior of F, Cl, Br and I: Implications for the fate of halogens during planetary accretion and the formation of magmatic ore deposits. *Geochimica et Cosmochimica Acta*, *273*, 275–290. https://doi.org/10.1016/j.gca.2020.01.006

Steenstra, E. S., Lin, Y., Dankers, D., Rai, N., Berndt, J., Matveev, S., & van Westrenen, W. (2017). The lunar core can be a major reservoir for volatile elements S, Se, Te and Sb. *Scientific Reports*, *7*(1), 14552. https://doi.org/10.1038/s41598-017-15203-0

Steenstra, E. S., Seegers, A. X., Putter, R., Berndt, J., Klemme, S., Matveev, S., Bullock, E. S., & Westrenen, W. van. (2020). Metal-silicate partitioning systematics of siderophile elements at reducing conditions: A new experimental database. *Icarus*, *335*, 113391. https://doi.org/10.1016/j.icarus.2019.113391

Steenstra, E. S., Trautner, V. T., Berndt, J., Klemme, S., & Westrenen, W. van. (2020). Trace element partitioning between sulfide-, metal- and silicate melts at highly reduced conditions: Insights into the distribution of volatile elements during core formation in reduced bodies. *Icarus*, *335*, 113408. https://doi.org/10.1016/j.icarus.2019.113408

Thibault, Y., & Walter, M. J. (1995). The influence of pressure and temperature on the metal-silicate partition coefficients of nickel and cobalt in a model C1 chondrite and implications for metal segregation in a deep magma ocean. *Geochimica et Cosmochimica Acta*, *59*(5), 991–1002. https://doi.org/10.1016/0016-7037(95)00017-8

Tuff, J., Wood, B. J., & Wade, J. (2011). The effect of Si on metal–silicate partitioning of siderophile elements and implications for the conditions of core formation. *Geochimica et Cosmochimica Acta*, *75*(2), 673–690. https://doi.org/10.1016/j.gca.2010.10.027

Wade, J., & Wood, B. J. (2001). The Earth's 'missing' niobium may be in the core. *Nature*, *409*(6816), 75–78. https://doi.org/10.1038/35051064

Wade, J., & Wood, B. J. (2005). Core formation and the oxidation state of the Earth. *Earth and Planetary Science Letters*, *236*(1), 78–95. https://doi.org/10.1016/j.epsl.2005.05.017

Walker, D., Norby, L., & Jones, J. H. (1993). Superheating Effects on Metal-Silicate Partitioning of Siderophile Elements. *Science*, *262*(5141), 1858–1861. https://doi.org/10.1126/science.262.5141.1858

Wood, B. J., Kiseeva, E. S., & Mirolo, F. J. (2014). Accretion and core formation: The effects of sulfur on metal–silicate partition coefficients. *Geochimica et Cosmochimica Acta*, *145*, 248–267. https://doi.org/10.1016/j.gca.2014.09.002

Wood, B. J., Wade, J., & Kilburn, M. R. (2008). Core formation and the oxidation state of the Earth: Additional constraints from Nb, V and Cr partitioning. *Geochimica et Cosmochimica Acta*, *72*(5), 1415–1426. https://doi.org/10.1016/j.gca.2007.11.036